Mucosal delivery of a double-stapled RSV peptide prevents nasopulmonary infection

Gregory H. Bird,[1,2] Sandhya Boyapalle,[3,4] Terianne Wong,[3,4,5] Kwadwo Opoku-Nsiah,[1] Raminder Bedi,[4] W. Christian Crannell,[1] Alisa F. Perry,[1] Huy Nguyen,[3] Viviana Sampayo,[3] Ankita Devareddy,[3] Subhra Mohapatra,[3,4,5] Shyam S. Mohapatra,[3,4] and Loren D. Walensky[1,2]

[1]Department of Pediatric Oncology and the Linde Program in Cancer Chemical Biology, Dana-Farber Cancer Institute, Boston, Massachusetts, USA. [2]Department of Pediatrics, Children's Hospital Boston, Harvard Medical School, Boston, Massachusetts, USA. [3]James A. Haley Veterans Administration Medical Center, Tampa, Florida, USA. [4]Nanomedicine Research Center and Division of Translational Medicine, Department of Internal Medicine, and [5]Department of Molecular Medicine, University of South Florida, Tampa, Florida, USA.

Respiratory syncytial virus (RSV) infection accounts for approximately 64 million cases of respiratory disease and 200,000 deaths worldwide each year, yet no broadly effective prophylactic or treatment regimen is available. RSV deploys paired, self-associating, heptad repeat domains of its fusion protein, RSV-F, to form a fusogenic 6-helix bundle that enables the virus to penetrate the host cell membrane. Here, we developed hydrocarbon double-stapled RSV fusion peptides that exhibit stabilized α-helical structure and striking proteolytic resistance. Pretreatment with double-stapled RSV peptides that specifically bound to the RSV fusion bundle inhibited infection by both laboratory and clinical RSV isolates in cells and murine infection models. Intranasal delivery of a lead double-stapled RSV peptide effectively prevented viral infection of the nares. A chitosan-based nanoparticle preparation markedly enhanced pulmonary delivery, further preventing progression of RSV infection to the lung. Thus, our results provide a strategy for inhibiting RSV infection by mucosal and endotracheal delivery of double-stapled RSV fusion peptides.

Introduction

New therapeutic strategies are needed to prevent and treat RSV infection, which causes significant morbidity and mortality worldwide each year (1). RSV can produce acute respiratory illness in patients of all ages, but strikes the age extremes, infants and the elderly, with highest frequency. RSV is a major, global cause of severe lower respiratory tract viral illness in infants and children, responsible for 70,000–126,000 infant hospitalizations for pneumonia or bronchiolitis and 400 infant deaths every year in the US alone (2, 3). The elderly are also at risk for severe disease (4, 5), with up to 62,000 RSV-associated hospitalizations reported annually in the US (6). RSV attack rates in US nursing homes are approximately 5%–10% per year, with a 2%–8% case fatality rate, amounting to approximately 10,000 deaths yearly among individuals older than 64 years (7).

A humanized monoclonal antibody against RSV-F, palivizumab, is the current mainstay for prophylaxis of children younger than 24 months who are at high risk of severe RSV infection, but is only moderately effective at preventing infection (8, 9). Although ribavirin, a nucleoside analog with modest in vitro activity against RSV, is FDA approved for the treatment of RSV infection, its routine use in infants and children is not recommended due to lack of proven efficacy (10). The morbidity and mortality associated with RSV infection have continued to invigorate efforts to develop peptide (11–13), small-molecule (14–18), DNA (19, 20), siRNA-based (21), and vaccine strategies (22–24) to combat RSV infection. For example, a RhoA-derived peptide, termed C3, was shown to inhibit the interaction between the RSV-F fusion protein and RhoA GTPase, thereby blocking syncytium formation. The small molecules RFI-641 (17) and VP-14637 (15) were reported to inhibit viral entry by targeting RSV-F. Despite a broad range of anti-RSV efforts, new FDA-approved drugs have yet to emerge. However, a recent breakthrough in the design of RSV-F glycoprotein stabilized to preserve a highly antigenic site in its prefusion state successfully yielded RSV-specific neutralizing antibodies in mice and macaques, providing new hope for an RSV vaccine (23, 25).

RSV is a member of the Paramyxoviridae family of viruses, which contain 3 glycoproteins on the viral envelope. The RSV-F surface protein mediates fusion of the RSV envelope with the host cell membrane (26). Like HIV-1, influenza, Ebola, and SARS viruses, the RSV fusion process requires formation of a 6-helix bundle (6-HB) that enables the virus to penetrate the host membrane (27). Initially, RSV-F exists as a core trimer composed of the N-terminal heptad repeat domain (NHR), upon which the C-terminal heptad repeat domain (CHR) folds back to form a hairpin turn, yielding an antiparallel trimer of dimers (14). The crystal structure of hRSV-F fragments confirmed the structural homology between the hRSV-F1 protein core and several other viral fusion proteins, including HIV-1 gp41, which suggests that therapeutic strategies designed to target HIV-1 viral fusion may be adapted to subvert RSV (26).

The peptidic drug enfuvirtide (T-20) contains the CHR sequence of HIV-1 gp41 and effectively targets gp41 in vivo, potently inhibiting HIV-1 fusion and entry (28). CHR peptides derived from RSV such as T118, which contains residues 488–522 of RSV-F, exhibited nanomolar inhibitory activity in RSV infectivity and syncytia formation assays (11). The mechanism of action mandates that T118 form an α-helical complex upon binding to the NHR tri-

Authorship note: Gregory H. Bird and Sandhya Boyapalle contributed equally to this work.

Conflict of interest: Loren D. Walensky is a scientific advisory board member and consultant for Aileron Therapeutics. Shyam S. Mohapatra is a scientific advisory board member for TransGenex Nanobiotech Inc.

Citation for this article: *J Clin Invest.* 2014;124(5):2113–2124. doi:10.1172/JCI71856.

meric core. However, T118 and other CHR derivatives exist primarily as random coils in solution, as evidenced by their less than 10% α-helical content (29). Thus, T118 and its analogs must pay the entropic cost of folding into the active conformation upon target binding, which translates into decreased binding affinity and biological activity. Furthermore, peptide unfolding renders the amide backbone highly susceptible to proteolytic degradation in vivo. Such liabilities have stifled the development of peptide-based RSV fusion inhibitors.

The poor pharmacologic properties of peptides have long motivated chemists to develop new synthetic strategies for stabilizing secondary structure so that the inherent potency and selectivity of peptides can be harnessed for targeting protein interactions. An important breakthrough in peptide α-helix stabilization derived from installing an all-hydrocarbon "staple" into native peptide sequence. Non-natural α,α-disubstituted amino acids bearing olefin tethers are substituted for natural amino acids at positions spanning 1 (*i,i*+4) or 2 (*i,i*+7) turns of the α-helix, followed by ruthenium-catalyzed olefin metathesis to effectively cross-link the inserted residues (30). The all-hydrocarbon constraint can confer α-helical structure, proteolytic stability, and improved biological activity by recapitulating bioactive structure (30, 31). Here we applied hydrocarbon stapling to develop stabilized α-helices of RSV-F (referred to herein as SAH-RSVF peptides) for evaluation as next-generation inhibitors of RSV infection (Figure 1A).

Results

Synthesis and binding activity of SAH-RSVF peptides. We previously explored the utility of inserting *i,i*+4 staples, which span 1 turn of an α-helix, into HR2 peptides derived from gp41, yielding a lead *i,i*+4 double-stapled peptide with optimized α-helical structure, proteolytic resistance, and anti–HIV-1 activity (32). By analogy, we installed single *i,i*+4 staples within the N- and C-terminal portions of an RSV HR2 peptide spanning residues 488–522, generating peptides SAH-RSVF$_a$–SAH-RSVF$_f$ (Supplemental Figure 1A; supplemental material available online with this article; doi:10.1172/JCI71856DS1). Circular dichroism analysis revealed that insertion of a single *i,i*+4 staple enhanced α-helical structure up to 2.3-fold over the unmodified SAH-RSVF peptide (Supplemental Figure 1B). To test for the capacity of the single *i,i*+4–stapled SAH-RSVF peptides to target the RSV fusion apparatus, we developed a recombinant 5-HB assay, as previously described for HIV-1 gp41 (33). The RSV 5-HB is composed of alternating HR1 and HR2 helices separated by short glycine/serine linkers. The corresponding recombinant DNA was synthesized as short overlapping oligonucleotides, assembled by PCR, and then subcloned into a vector containing a C-terminal hexahistidine tag. Recombinant 5-HB protein was expressed as inclusion bodies, and, after denaturing lysis, nickel affinity chromatography, dialysis, and protein refolding, yields of 10 mg/l were achieved. The fluorescently labeled RSVF template peptide directly bound to the RSV 5-HB with a K_D of 63 nM, as measured by fluorescence polarization (FP) assay (Supplemental Figure 1C), completing the formation of an RSV 6-HB (Supplemental Figure 1D), which was then deployed in competition FP binding assays. Comparative binding analyses revealed that single *i,i*+4–stapled SAH-RSVF peptides either matched (SAH-RSVF$_a$–SAH-RSVF$_c$ and SAH-RSVF$_e$) or exhibited weaker (SAH-RSVF$_d$ and SAH-RSVF$_f$) competitive binding activity than that of the unlabeled RSVF template peptide (Supplemental Figure 1E). To determine whether an equipotent binder could target native RSV virus, we conducted colocalization imaging analyses of A549 cells treated with FITC–SAH-RSVF$_b$ and RSV-A2 virus. Both live confocal microscopy and immunoelectron microscopy documented striking colocalization of peptide and virus, visualized as punctate structures at the plasma membrane (Supplemental Figure 2, A and B). Thus, SAH-RSVF$_b$, which bound to recombinant RSV 5-HB in vitro, likewise engaged native RSV in the setting of viral infection.

In an effort to improve upon the binding affinity of the unmodified SAH-RSVF peptide, we explored the effect of structural stabilization by use of *i,i*+7 staples, which cross-link a 2-turn span of α-helical peptide. A panel of N- and C-terminally *i,i*+7–stapled RSV peptides, designated SAH-RSVF$_A$–SAH-RSVF$_F$, were successfully synthesized (Figure 1B) and exhibited up to 3-fold stabilization of α-helical structure, as determined by circular dichroism (Figure 1C). In contrast to the *i,i*+4 series, the majority of *i,i*+7 single-stapled peptides showed notably enhanced competitive binding activity for RSV 5-HB compared with the unmodified peptide (Figure 1D). Interestingly, for those constructs with impaired binding activity, the degree of impairment correlated with progressive encroachment of the staple on the critical hydrophobic binding interface. Thus, for the RSVF template, 2-turn helix stabilization by *i,i*+7 stapling markedly enhances binding affinity for the RSV 5-HB.

Enhanced α-helicity and protease resistance of i,i+7 double-stapled SAH-RSVF peptides. We combined the best N- and C-terminal *i,i*+7 single-stapled peptides, in addition to carrying forward the nonbinding C-terminal F staple position as a negative control, to generate a series of *i,i*+7 double-stapled constructs (Figure 2A). In each case, the *i,i*+7 double-stapled peptides exhibited additive enhancement in α-helical content compared with the corresponding single-stapled analogs (Figure 2B), which suggests that double stapling in this context optimally reinforces α-helical structure throughout the length of the SAH-RSVF peptide. Of the *i,i*+7 double-stapled constructs, SAH-RSVF$_{BD}$ and SAH-RSVF$_{CD}$ retained the most potent competitive binding activity, followed by SAH-RSVF$_{BE}$ and SAH-RSVF$_{CE}$, and the predictably poor SAH-RSVF$_{BF}$ and SAH-RSVF$_{CF}$ analogs that contained the disruptive F staple (Figure 2C).

An important optimization criterion for peptide therapeutics is protease resistance. To measure the comparative protease susceptibility of unmodified and *i,i*+7 single- and double-stapled peptides, we subjected the lead SAH-RSVF constructs and their negative controls to trypsin digestion, followed by liquid chromatography/mass spectrometry (LC/MS) analysis of the reaction products over time. Whereas *i,i*+7 single stapling conferred up to 4-fold enhancement in peptide half-life compared with the unmodified peptide, *i,i*+7 double-stapled analogs manifested 3- to 33-fold improvement in proteolytic resistance (Figure 2D). In each case, the double-stapled peptides displayed at least additive proteolytic resistance of the corresponding single-stapled peptides, with synergistic benefit typically observed. We further subjected one of our lead RSV 5-HB competitive binders (SAH-RSVF$_{BD}$), its corresponding single-stapled analogs (SAH-RSVF$_B$ and SAH-RSVF$_D$), and a control panel (SAH-RSVF$_F$ and SAH-RSVF$_{BF}$) to even more aggressive proteolytic conditions using proteinase K, and again found striking proteolytic resistance of both double-stapled peptides compared with the corresponding single-stapled peptides and unmodified RSVF template (Figure 2E). Taken together, these data demonstrated that *i,i*+7 double stapling optimizes α-helicity and protease resistance, yielding structurally stable and high-affinity competitive inhibitors of RSV 6-HB formation.

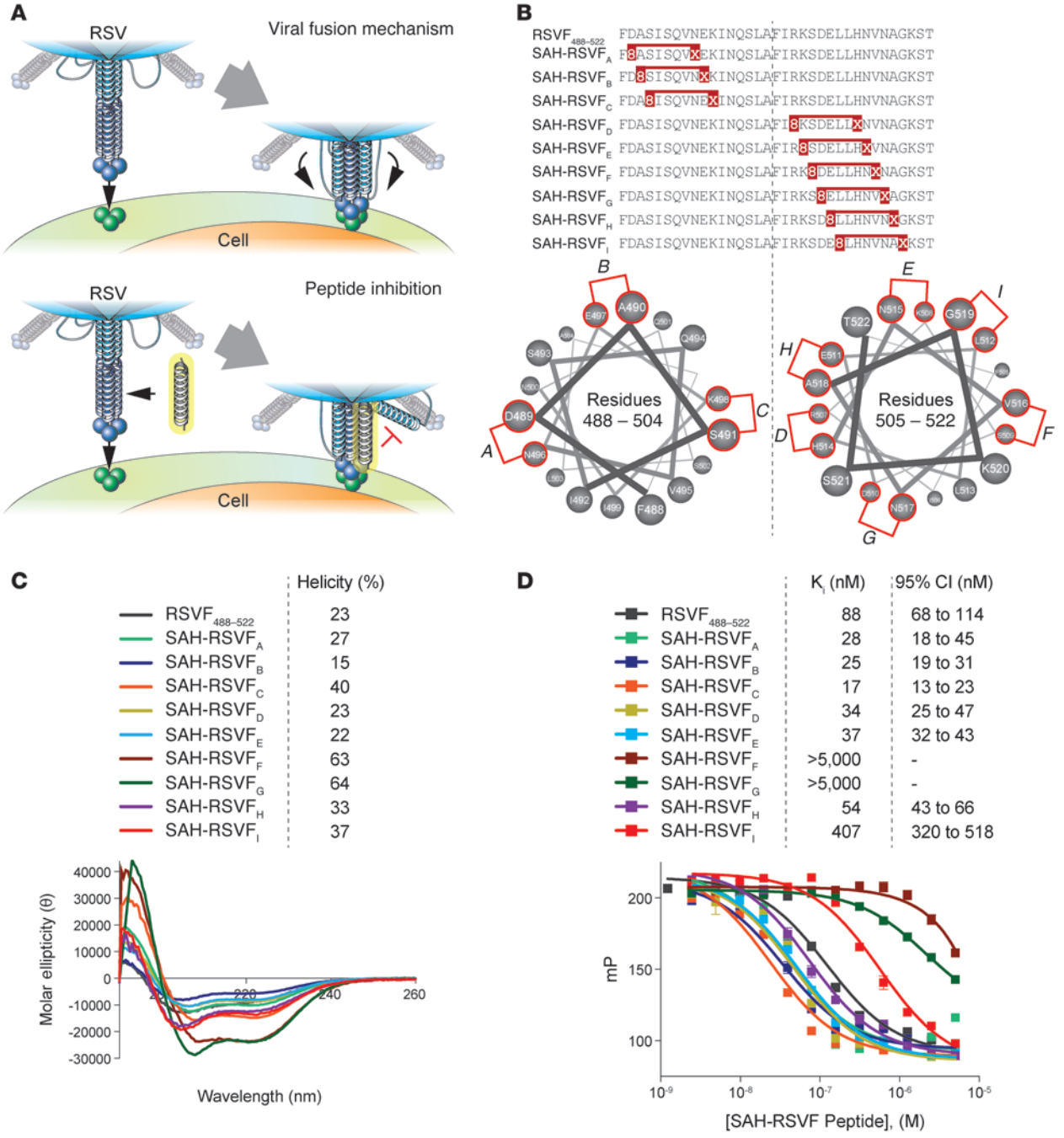

Figure 1

Design, α-helicity, and 5-HB binding activity of *i,i*+7–stapled SAH-RSVF peptides. (**A**) RSV fusion mechanism and its disruption by a decoy HR2 helix. (**B**) Sequence compositions and staple placement of *i,i*+7–stapled SAH-RSVF peptides. (**C**) Circular dichroism analysis of *i,i*+7–stapled SAH-RSVF peptides, demonstrating the observed range of α-helical stabilization by hydrocarbon stapling. (**D**) Competitive binding activity of *i,i*+7–stapled SAH-RSVF peptides against the FITC-RSVF/5-HB interaction. Data represent mean ± SEM for experiments performed in triplicate.

SAH-RSVF peptides inhibit RSV infectivity in vitro. To determine whether the 5-HB–targeting capability of *i,i*+7 single- and double-stapled peptides correlated with functional blockade of RSV infection, we pretreated A549 cells with vehicle or 5-μM concentrations of unmodified or *i,i*+7–stapled peptide, followed by infection with a recombinant GFP-expressing RSV (rgRSV). After a 1-hour infection period, the medium was replaced with fresh peptide-containing medium, and cells were incubated for an additional 24 hours, followed by harvesting for determination of percent GFP$^+$ cells by flow cytometry. Consistent with 5-HB binding avidity, SAH-RSVF$_B$, SAH-RSVF$_C$, SAH-RSVF$_D$, SAH-RSVF$_{BD}$, and SAH-RSVF$_{CD}$ demonstrated potent suppression of rgRSV infection, whereas all constructs containing the negative control F staple were even less effective at inhibiting infectivity than the unmodified SAH-RSVF

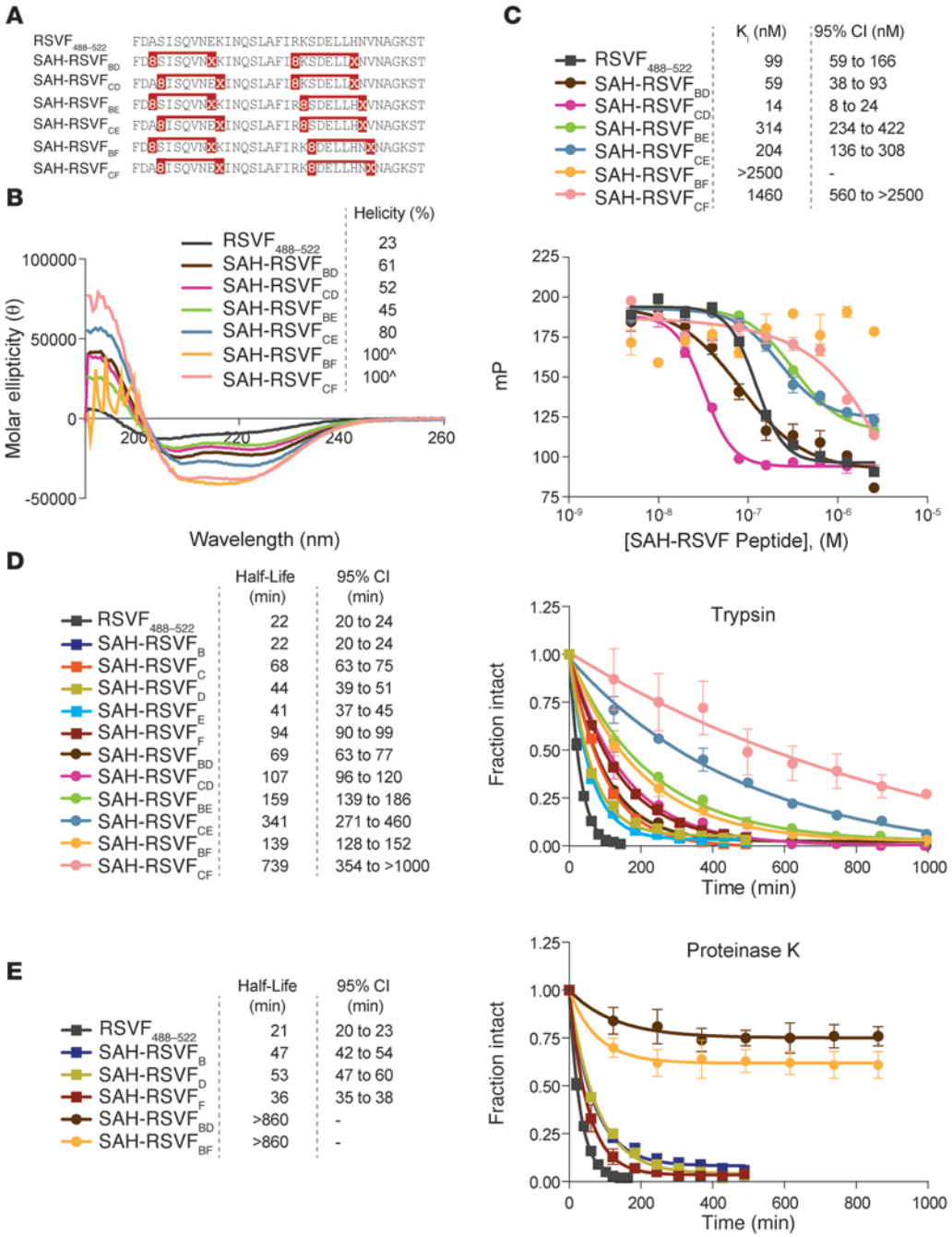

Figure 2

Design, α-helicity, 5-HB binding activity, and protease resistance of *i,i*+7 double-stapled SAH-RSVF peptides. (**A**) Sequence compositions and staple placement of *i,i*+7 double-stapled SAH-RSVF peptides. (**B**) Circular dichroism analysis of *i,i*+7 double-stapled SAH-RSVF peptides, demonstrating enhanced α-helical stabilization compared with the corresponding *i,i*+7 single-stapled peptides. ^, exceeds the calculated ideal α-helicity of an undecapeptide standard. (**C**) Competitive binding activity of *i,i*+7 double-stapled SAH-RSVF peptides against the FITC-RSVF/5-HB interaction. SAH-RSVF$_{BD}$ and SAH-RSVF$_{CD}$ were among the most effective competitive binders, whereas the negative control constructs SAH-RSVF$_{BF}$ and SAH-RSVF$_{CF}$ showed substantially impaired 5-HB binding activity. Data represent mean ± SEM for experiments performed in triplicate. (**D**) Trypsin resistance profile of *i,i*+7 single- and double-stapled SAH-RSVF peptides. (**E**) Proteinase K resistance profile of an exemplary subpanel of *i,i*+7 single- and double-stapled SAH-RSVF peptides. Data (mean ± SEM) represent fraction intact for experiments performed in triplicate.

peptide (Figure 3A and Supplemental Figure 3A). Correspondingly, the 3 best inhibitors of rgRSV infection, SAH-RSVF$_{B}$, SAH-RSVF$_{C}$, and SAH-RSVF$_{BD}$, were most effective at blocking viral syncytia formation, with those analogs containing the F staple again showing no inhibitory activity (Figure 3B). Next, the lead double-stapled peptides, SAH-RSVF$_{BD}$ and SAH-RSVF$_{CD}$, along with their negative controls, SAH-RSVF$_{BF}$ and SAH-RSVF$_{CF}$, were subjected to RSV-A2 plaque assay and viral titer measurement. A549 cells were treated with vehicle or 5 μM stapled peptide as above, except that cells were infected with RSV-A2 for a 2-hour period. The cells and media were harvested after 24 hours of incubation in fresh peptide-containing medium. Cells were analyzed for RSV-N mRNA levels, and the collected supernatant was applied to HEp-2 cells for plaque assay and measurement of viral titers after 5 days. Whereas SAH-RSVF$_{BF}$ and SAH-RSVF$_{CF}$ treatment had no suppressive effect on RSV-A2 viral titers or RSV-N mRNA levels compared with the untreated control, SAH-RSVF$_{BD}$ and SAH-RSVF$_{CD}$ peptides significantly reduced both viral titers and RSV-N transcript levels, with SAH-RSVF$_{BD}$ manifesting the most potent inhibitory activity (Figure 3C and Supplemental Figure 4). To confirm the efficacy of SAH-RSVF$_{BD}$, plaque assay and viral titer measurements were repeated using 30 minutes of peptide pretreatment followed by infection with both lab and clinical RSV isolates, including RSV-A2, RSV 2-20, and the recombinant RSV-A2 strain express-

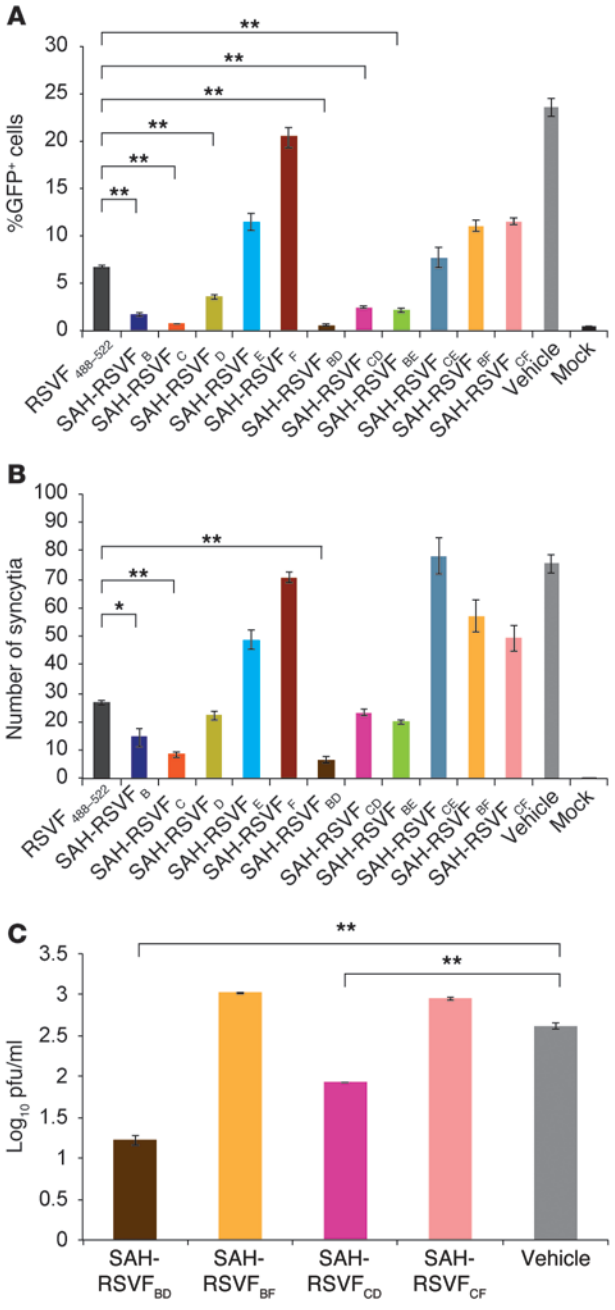

Figure 3

Inhibition of RSV infection and syncytia formation by *i,i*+7–stapled SAH-RSVF peptides. (**A**) The capacity of SAH-RSVF peptides to suppress infection of A549 cells by GFP-expressing rgRSV correlated with their competitive binding potency in the 5-HB FP assay (see Figure 1D and Figure 2C). SAH-RSVF$_B$, SAH-RSVF$_C$, SAH-RSVF$_D$, SAH-RSVF$_{BD}$, and SAH-RSVF$_{CD}$ demonstrated the most robust viral inhibitory activity, whereas controls SAH-RSVF$_F$, SAH-RSVF$_{BF}$, and SAH-RSVF$_{CF}$ were markedly impaired. Data represent mean ± SEM for experiments performed in triplicate. (**B**) Comparative activity of SAH-RSVF peptides in inhibiting syncytia formation after rgRSV infection of A549 cells, as counted in 3 different wells at 4 discrete locations per well at 48 hours after infection. Data are mean ± SEM. (**C**) Inhibition of RSV-A2 infection by SAH-RSVF peptides, as assessed by HEp-2 cell plaque assay and measurement of viral titers (pfu/ml). Data are mean ± SEM for 2 independent experiments performed in technical triplicates. (**D**) SAH-RSVF$_{BD}$ prevented viral infection of A549 cells by RSV-A2, RSV 2-20, and RSV-rA2Line19F, as assessed by HEp-2 cell plaque assay and measurement of viral titers (pfu/ml). Data are mean ± SEM for 2 independent experiments performed in technical triplicates. $^*P < 0.001$, $^{**}P < 0.0001$.

ing fusion protein from clinical isolate Line 19 (RSV-rA2Line19F) (34). In each case, SAH-RSVF$_{BD}$ showed marked suppression of viral titers compared with the vehicle control (Figure 3D). Finally, we applied the method of Saika et al. (35) to confirm that SAH-RSVF$_{BD}$–mediated inhibition of RSV infectivity indeed derived from blockade of viral fusion with the cell membrane. RSV-A2 virus was labeled with the fluorescent lipids R18 (red) and DiOC18 (green) and applied to A549 cells. Labeled virus is initially red due to the quenching of the DiOC18 fluorescent signal by R18; upon fusion with cellular membrane, the lipids are diluted, and dequenching of DiOC18 is reflected by the shift in red coloration to orange-yellow or green, as imaged by confocal microscopy. We found that SAH-RSVF$_{BD}$ treatment (5 μM) reduced the number of RSV-A2 fusion events by 60% (Supplemental Figure 5), highlighting the mechanistic basis for peptide activity.

Intranasal pretreatment with SAH-RSVF$_{BD}$ blocks nasal and pulmonary RSV infection. To determine whether the in vitro anti-RSV activity of SAH-RSVF$_{BD}$ translated to an in vivo context, we administered vehicle, SAH-RSVF$_{BD}$, or SAH-RSVF$_{BF}$ by nasal drop (50 μl of 125 μM solution in 1.2% DMSO) to 10-week-old BALB/c mice (n = 4 per cohort) followed by intranasal inoculation with a single dose of rgRSV (1×10^6 pfu) 1 hour later. Mice were sacrificed 24 hours after infection, and noses were harvested, sectioned, stained with DAPI, and subjected to fluorescence imaging. The microscopic images demonstrated a marked reduction in GFP$^+$ nasal tissue in SAH-RSVF$_{BD}$–treated mice, whereas SAH-RSVF$_{BF}$ showed no such

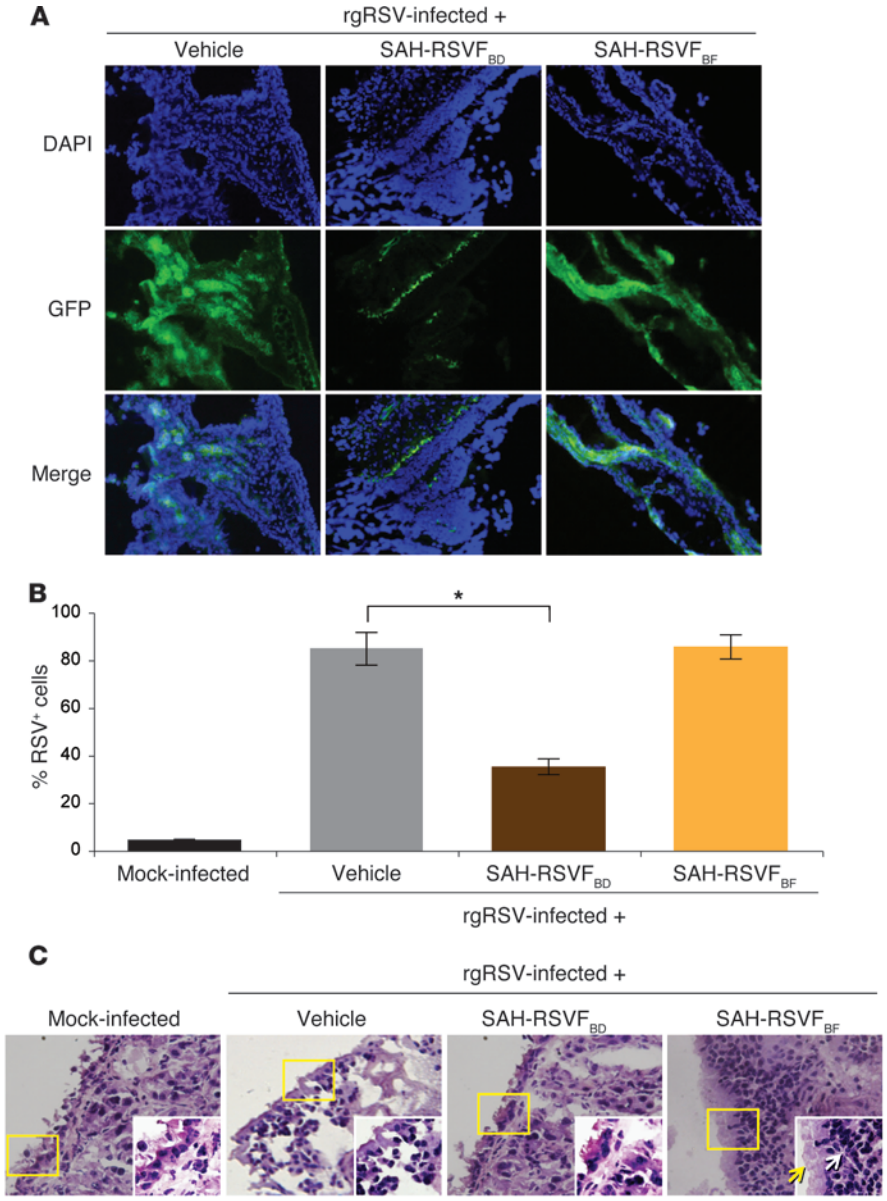

Figure 4
Inhibition of nasal RSV infection by intranasal pretreatment with SAH-RSVF$_{BD}$. (**A**) 10-week-old BALB/c mice were treated with vehicle (1.2% DMSO) or the indicated SAH-RSVF peptides (50 μl of 125 μM solution in 1.2% DMSO) by nasal drop, followed by inoculation with rgRSV (1 × 10^6 pfu/mouse). Tissues were harvested 24 hours after infection and processed for fluorescence imaging, which revealed marked suppression of GFP positivity by SAH-RSVF$_{BD}$, but not the control SAH-RSVF$_{BF}$. Original magnification, ×20. (**B**) Average GFP positivity, quantified by ImageJ analysis of 8 images (4 sections) per mouse. Data (mean ± SEM) represent percent GFP$^+$ of total DAPI$^+$ cells. (**C**) H&E staining of the nasal sections demonstrated airway constriction from mucous production (a disease hallmark in mice; yellow arrow) and inflammation (mononuclear cell infiltrates; white arrow) in rgRSV-infected mice treated with vehicle and SAH-RSVF$_{BF}$, but notably less airway constriction and immune cell infiltration in SAH-RSVF$_{BD}$–treated mice. Sections from mock-infected mice served as a negative control for nasal mucosal inflammation. Insets show magnified views of yellow boxed regions. Original magnification, ×20; ×40 (insets). *P < 0.001.

effect (Figure 4A). Quantitation of GFP positivity by ImageJ analysis demonstrated a statistically significant reduction in nasal tissue fluorescence of greater than 50% compared with that from mice treated with vehicle or SAH-RSVF$_{BF}$ (Figure 4B), demonstrative of significantly reduced RSV infection. H&E staining of the nose sections revealed thickened mucosa and inflammation in rgRSV-infected mice treated with vehicle or SAH-RSVF$_{BF}$ (Figure 4C). In contrast, rgRSV-infected mice treated with SAH-RSVF$_{BD}$ showed little to no inflammation, with nasal histology appearing similar to that of mock-infected animals (Figure 4C). Thus, pretreatment of rgRSV-infected mice with intranasal SAH-RSVF$_{BD}$ markedly decreases nasal infection in a sequence-dependent manner.

As nasal RSV infection can spread to the lungs and cause bronchiolitis and pneumonia, we sought to determine whether intranasal SAH-RSVF$_{BD}$ could likewise suppress the development of pulmonary RSV infection in mice using established models (21, 36–38). Vehicle, SAH-RSVF$_{BD}$, or SAH-RSVF$_{BF}$ were administered by nasal drop (50 μl of 125 μM solution in 1.2% DMSO) to 10-week-old BALB/c mice (n = 4 per cohort), followed by intranasal inoculation with RSV-A2 (1 × 10^6 pfu) 1 hour later. 4 days later, mice were sacrificed, the lungs were subjected to 4% paraformaldehyde perfusion, and left lung lobes were harvested for cryopreservation, sectioning, and anti-RSV immunofluorescence microscopy. The immunofluorescence images demonstrated a marked reduction in RSV antigen in the lung tissue of SAH-RSVF$_{BD}$–treated mice, whereas the level of RSV detection in SAH-RSVF$_{BF}$–treated mice was as robust as that of vehicle-treated mice (Figure 5A). ImageJ analysis documented that SAH-RSVF$_{BD}$ treatment reduced RSV immunofluorescence more than 70% compared with that observed for mice treated with vehicle or SAH-RSVF$_{BF}$ (Figure 5B). We further generated homogenates from the cranial lobe of the right lungs of mice and subjected the supernatants to viral titer determination by HEp-2 cell plaque assay. Again, only the lung homogenates harvested from SAH-RSVF$_{BD}$–treated mice

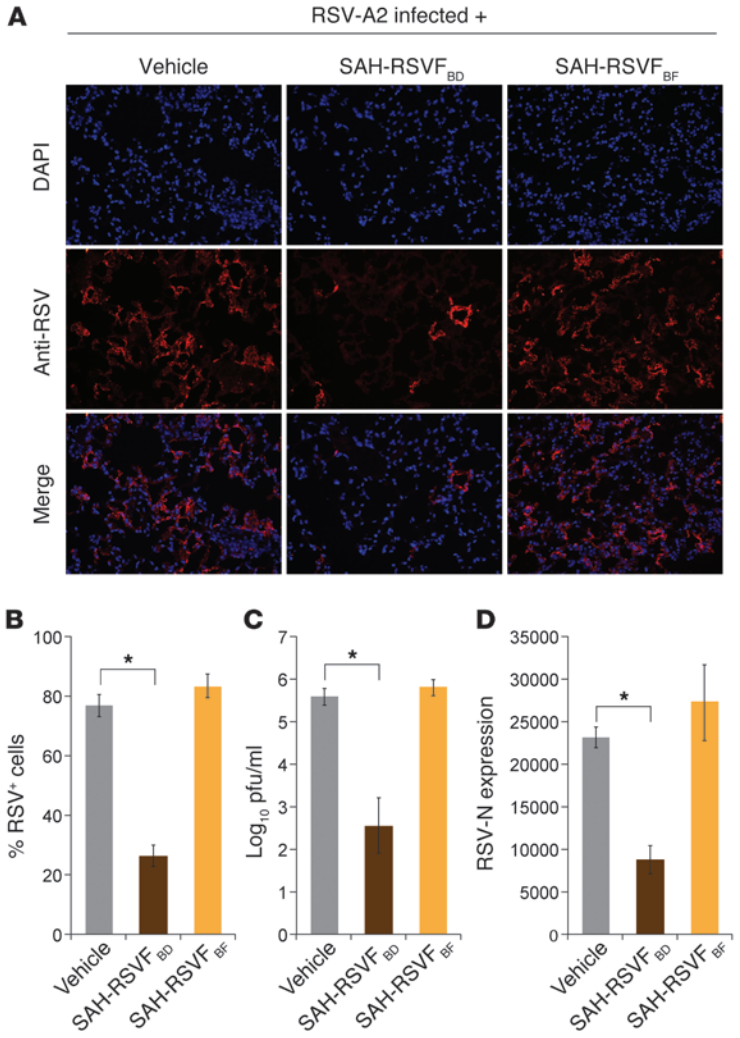

Figure 5

Intranasal prophylaxis with SAH-RSVF$_{BD}$ inhibits spread of RSV infection to the lung. (**A**) Anti-RSV immunofluorescence microscopy of lung sections from 10 week-old BALB/c mice treated with vehicle and SAH-RSVF peptides (50 μl of 125 μM solution in 1.2% DMSO) followed by intranasal RSV-A2 inoculation (1×10^6 pfu/mouse) after 1 hour and sacrifice 4 days later. Original magnification, ×20. (**B**) Average RSV positivity (red) by ImageJ analysis of 8 images (4 sections) per mouse. RSV$^+$ cells are expressed as a percentage of total DAPI$^+$ cells (mean ± SEM). (**C**) Viral titers ($\log_{10}$ pfu/ml) were measured in the supernatants of lung homogenates by HEp-2 plaque assay. Data are mean ± SEM. (**D**) Total RNA was isolated from the lungs (right caudal lobe) of treated mice, and RSV-N expression was quantitated by RT-PCR. Data are mean ± SEM. *$P < 0.0001$.

exhibited reduced viral titers (Figure 5C). Finally, we extracted total RNA from the caudal lobe of the right lungs and performed quantitative RT-PCR for the RSV-N transcript. Compared with tissue from mock-infected mice, RSV-A2 inoculation led to a robust increase in RSV-N expression. Whereas RSV-N expression levels in lung tissue from vehicle- and SAH-RSVF$_{BF}$–treated mice were similarly elevated, SAH-RSVF$_{BD}$ treatment reduced expression levels by approximately 65% (Figure 5D). The experiment was also performed with peptide dosing and viral reinoculation 16 hours after the first infection (n=3 per cohort), and similar sequence-dependent inhibitory effects of SAH-RSVF$_{BD}$ were observed (Supplemental Figure 6). Thus, by each measure, prophylactic intranasal treatment with SAH-RSVF$_{BD}$ effectively reduced both upper and lower respiratory infection by RSV.

Prophylactic intratracheal treatment with a nanoparticle preparation of SAH-RSVF$_{BD}$ blocks pulmonary RSV infection. Although local pretreatment with SAH-RSVF$_{BD}$ at the intranasal site of RSV infection reduced nasal infection and subsequent spread to the lungs, we next sought to determine whether peptide delivery to the lung via the intratracheal route could prevent the natural progression of RSV infection after intranasal inoculation. To assess and potentially augment lung tissue exposure, we generated a chitosan-based nanoparticle (NP) (21) preparation of Cy5-labeled SAH-RSVF$_{BD}$ (100 μM peptide, 1:2.5 peptide/NP ratio, 50 μl volume) and compared lung tissue fluorescence 24 hours after intratracheal administration of vehicle, Cy5-labeled SAH-RSVF$_{BD}$ peptide alone, or the corresponding NP preparation. With both peptide treatments, lung tissue sections demonstrated robust fluorescence, but specimens from mice treated with the NP preparation exhibited more uniform and higher-level delivery, as assessed by confocal microscopy and ImageJ analysis (Figure 6, A and B). These data suggest that pharmacologic approaches to concentrating and retaining SAH-RSVF$_{BD}$ at the pulmonary mucosal surface may be an effective means of maximizing its therapeutic potential.

To measure the capacity of SAH-RSVF$_{BD}$ to confer anti-RSV prophylaxis for a prolonged period when administered by the intratracheal route, we pretreated mice ($n = 3$ per cohort) with vehicle, SAH-RSVF$_{BD}$, or the corresponding NP preparation, followed by a single intranasal inoculation with RSV-rA2Line19F (1×10^6 pfu/mouse) or mock infection 48 hours later. Anti-RSV immunofluorescence confocal microscopy of the lung revealed a striking near absence of lung tissue fluorescence in infected mice pretreated with the NP preparation of SAH-RSVF$_{BD}$, whereas no statistically significant effects were observed by ImageJ analysis for mice treated with SAH-RSVF$_{BD}$ or NPs alone (Figure 6, C and D). Consistent with these imaging data, only the lung homogenates from mice treated with the NP preparation of SAH-RSVF$_{BD}$ demonstrated marked reduction of viral titers, by HEp-2 cell plaque assay, and RSV-N expression, by quantitative RT-PCR (Figure 6, E and F). We repeated the experiment ($n = 3$ per cohort) with an extended 72-hour prophylactic window and obtained nearly identical results, with striking protection against RSV infection by the NP preparation of SAH-RSVF$_{BD}$ (Supplemental Figure 7). Thus, for intratracheal administration of SAH-RSVF$_{BD}$ in the context of 48- and 72-hour intervals between peptide prophylaxis and intranasal viral inoculation, the higher-level tissue exposure conferred by the NP preparation of SAH-RSVF$_{BD}$ effectively suppressed the spread of RSV infection to the lung.

Discussion

New technologies that fortify lengthy peptides, such as hydrocarbon double stapling, are reinvigorating efforts to optimize natural peptides for therapeutic application. Indeed, the fusion domain helices of a variety of pathogenic viruses, including RSV, Ebola, SARS, and influenza, may hold the key to a series of next-generation inhibitors of viral infections. The pioneering agent,

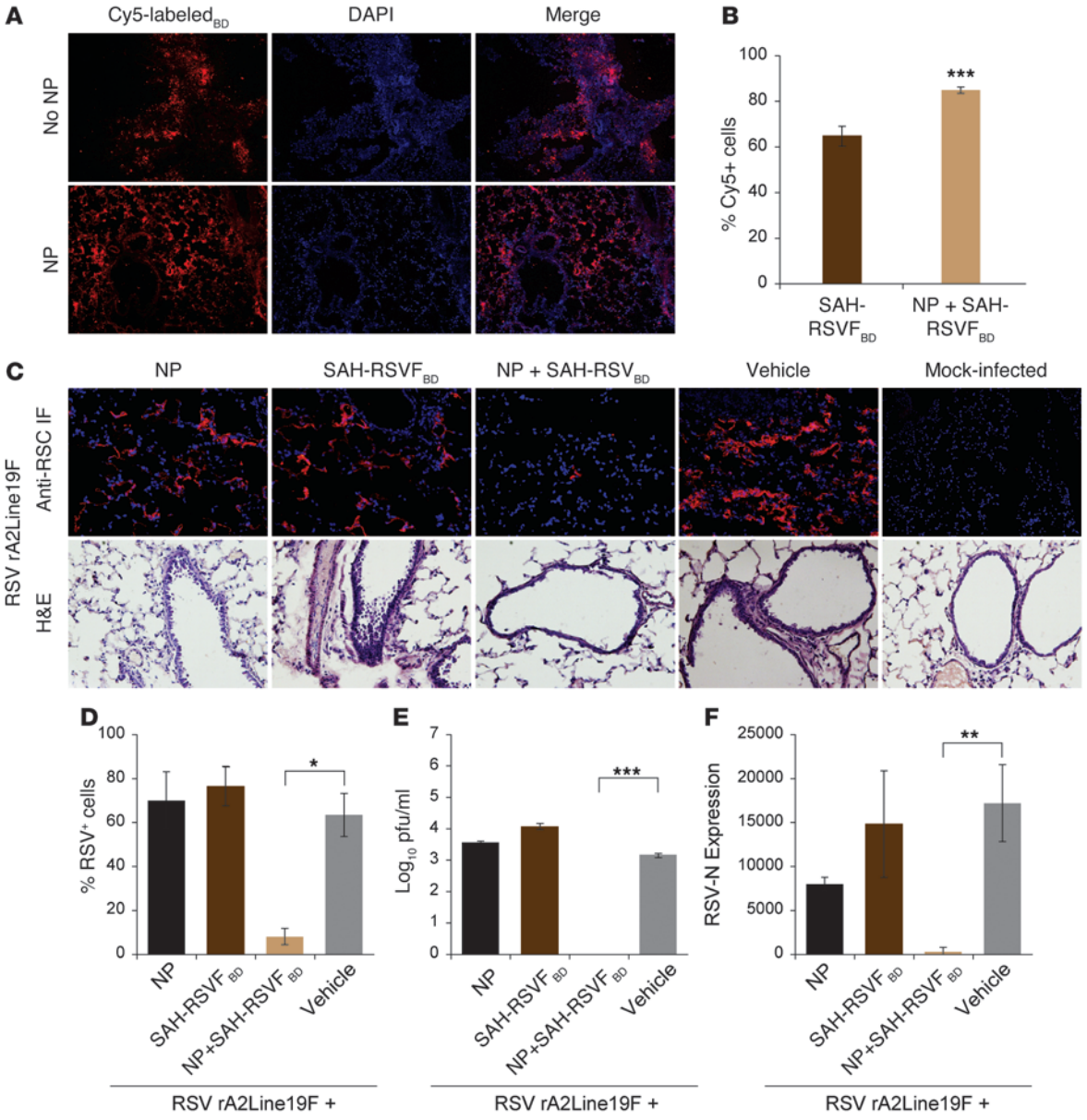

Figure 6

Intratracheal SAH-RSVF$_{BD}$ as a NP preparation inhibits pulmonary RSV infection. (**A**) 10-week-old BALB/c mice were treated intratracheally with vehicle or Cy5-labeled SAH-RSVF$_{BD}$ administered alone (100 μM) or in combination with NPs (1:2.5 peptide/NP ratio) in a 50-μl volume. Mice were sacrificed 24 hours after treatment, and lungs were harvested after 1% paraformaldehyde perfusion, followed by cryopreservation in OCT. Sections (5 μm) were mounted in DAPI-containing medium and imaged with an Olympus fluorescent microscope. Original magnification, ×20. (**B**) ImageJ analysis was used to quantify Cy5$^+$ cells, expressed as a percentage of total DAPI$^+$ cells. Data represent mean ± SEM. (**C**) 10-week-old BALB/c mice were treated intratracheally with 50 μl NP, SAH-RSVF$_{BD}$ (250 μM peptide in 1.2% DMSO), the combination (1:2.5 peptide/NP ratio), or vehicle. 48 hours after treatment, mice were inoculated intranasally with single dose recombinant RSV-rA2Line19F (1×10^6 pfu/mouse). Control mice received 50 μl vehicle intratracheally followed by mock inoculation 48 hours later. Mice were sacrificed 4 days after infection, and 5-μm sections from 1% paraformaldehyde-perfused and fixed lungs were subjected to anti-RSV immunofluorescence (IF) analysis and H&E staining. Lung tissue from mice treated with the SAH-RSVF$_{BD}$/NP formulation demonstrated decreased inflammatory cell infiltrates. Original magnification, ×20. (**D**) Average RSV positivity (red), quantified by ImageJ analysis of 8 images (4 sections) per mouse. GFP$^+$ cells are expressed as a percentage of total DAPI$^+$ cells. (**E**) Viral titers ($\log_{10}$ pfu/ml) in the supernatants of lung homogenates, measured by HEp-2 plaque assay. (**F**) Total RNA was isolated from the lungs of treated mice, and RSV-N expression was quantitated by RT-PCR. All data are mean ± SEM. *$P < 0.01$, **$P < 0.001$, ***$P < 0.0001$.

enfuvirtide, demonstrated bona fide therapeutic activity against HIV-1 with a compelling mechanism of action (28). Although still prescribed in the context of multidrug-resistant HIV-1 infection, its utility has been far outpaced by the extensive arsenal of alternative and highly effective anti–HIV-1 agents with oral bioavailability. The large doses (and attendant costs) of enfuvirtide required to achieve inhibitory activity, along with the twice-daily subcutaneous mode of administration, are a direct consequence of the structural instability and proteolytic susceptibility of lengthy peptides. However, with recent advances in conformational control of peptides, including the advancement of peptide double stapling to address traditional peptide liabilities (32), the antiviral activity of natural α-helical peptide interaction domains implicated in viral fusion warrant a second look, especially when treatment options for specific viruses are scarce.

Here, we found that the insertion of 2 *i,i*+7 staples (each spanning 2 turns of an α-helix) into the peptide sequence of the HR2 domain of RSV yielded a lead peptide with enhanced structure in solution, striking protease resistance, and the capacity to block infection by laboratory and clinical RSV isolates in vitro and in vivo. Following our previously reported design principles for the development of stapled peptides for biomedical research (39), we explored (a) differential hydrocarbon staple compositions, including *i,i*+4 and *i,i*+7 staples; (b) the comparative benefits of single versus double stapling in the context of a lengthy peptide template; and, importantly, (c) the biophysical and biological effect of alternative placement of staples within the peptide sequence. Disruption of the binding interface by staple F exemplifies the importance of preserving key peptide/target interactions. In addition, disruptive staple positions provide mutant controls for verifying the specificity and sequence dependence of lead construct bioactivity. By vetting SAH-RSVF$_{BD}$ in a comprehensive battery of assays, spanning biochemical, cellular, and in vivo analyses, we demonstrate proof of concept for the potential therapeutic utility of SAH-RSVF peptides in blocking both the intranasal establishment and the pulmonary spread of RSV infection.

Having applied all-hydrocarbon stapling to 2 viral fusion peptides with distinct amino acid sequences, but common mechanisms of action (32), we noted the emergence of several general trends that may inform the broader applicability of the approach. First, we found that scanning with *i,i*+4 and *i,i*+7 staples was a key first step in determining the optimal type and placement of hydrocarbon staples for a given peptide template. Second, double stapling was markedly superior to single stapling in enforcing the structure and protease resistance of such lengthy peptides. Third, a battery of correlative in vitro and cellular structure-function assays was essential to selecting lead constructs for in vivo testing. Finally, the sequence-dependent results observed in cells and in vivo, facilitated by the use of negative control constructs with point mutants or disruptive staples, was critical for validating on-mechanism biological activity. The capacity to generate both anti–HIV-1 and anti-RSV double-stapled peptides that blocked viral infection by fusion inhibition suggests that all-hydrocarbon stapling may be a general approach for developing antivirals for the Paramyxoviridae family.

We combined peptide stapling and NP delivery technologies, for the first time to our knowledge, in an effort to maximize tissue delivery and persistence. In the context of antiviral prophylaxis, the capacity of NPs to concentrate the therapeutic agent at the site of viral infection, coupled with the structural stability and protease resistance conferred by peptide stapling, yielded a dramatic suppression of viral infection not achieved under the same experimental conditions by the stapled peptide alone. The observed prevention of pulmonary spread of nasal RSV infection by intratracheally administered SAH-RSVF$_{BD}$–coated polysaccharide NPs correlated with higher-level and more uniform distribution of Cy5-labeled peptide, and with suppression of RSV infection, by 3 measures: viral imaging, viral titers, and RSV-N expression in lung specimens. Thus, hydrocarbon double-stapled SAH-RSVF peptides may provide a new pharmacologic opportunity to combat RSV infection, while also serving as a paradigm for extending the utility of peptide stapling technology to other undrugged viruses that share this fusion mechanism. Key next steps toward translation include expanding preclinical in vivo testing to define and optimize (a) the maximal duration of prophylaxis and (b) the efficacy in mitigating established infection. Given the documented neutralizing immunogenicity of RSV-F epitopes (23, 25), the capacity of SAH-RSVF exposure to elicit neutralizing antibodies for potential vaccine development is also worthy of exploration.

Methods

Peptide synthesis. SAH-RSVF peptides were generated by automated peptide synthesis (Aapptec Apex 396) using Fmoc-protected natural amino acids (Advanced ChemTech), (*S*)-2-(((9*H*-fluoren-9-yl)methoxy) carbonylamino)-2-methyl-hept-6-enoic acid (*R*)-2-(((9*H*-fluoren-9-yl) methoxy)carbonylamino)-2-methyl-dec-9-enoic acid (Nagase Chemical), and Rink amide resin (Novabiochem). Upon completion of automated synthesis, the N terminus was either acetylated or capped with Fmoc-β-Ala for FITC or Cy5 derivatization. To generate hydrocarbon staples by olefin metathesis, the resin was charged with a 10-mM solution of bis(tricyclohexylphosphine)-benzylidene ruthenium (IV) dichloride (Grubbs' first-generation catalyst) in 1,2-dichloroethane and stirred for 2 hours, followed by repeating the reaction twice as described with fresh catalyst. For FITC and Cy5 derivatization, Fmoc-β-Ala was deprotected with piperidine in N-methylpyrrolidone (NMP) and then reacted with FITC or Cy5 NHS ester (Lumiprobe) (3 eq relative to resin-bound amine) and triethylamine (3 eq) in dimethylformamide overnight. The peptide was cleaved from the resin and deprotected in 95% TFA, 2.5% triisopropyl silane (TIS), and 2.5% water, and then precipitated with diethylether/hexanes. SAH-RSVF peptides were purified by reverse-phase HPLC (Agilent) using a C18 column (Zorbax), characterized by LC/MS (mass spectra obtained using electrospray in positive ion mode), and quantified by amino acid analysis on an Agilent high-performance amino acid analyzer. Working stock solutions were generated by dissolving the lyophilized powder in 100% DMSO at 1–10 mM. SAH-RSVF powder and DMSO solutions were stored at –20°C.

Circular dichroism. CD spectra were recorded on an Aviv Biomedical spectrometer (Model 410) equipped with a Peltier temperature controller, 1-mm path-length cells, and a thermoelectric sample changer with 5-position rotor, scanning 190–260 nm in 0.5-nm increments with a 0.5-second averaging time. Peptides were dissolved in 5 mM potassium phosphate (pH 7.5) to a final concentration of 50 μM. Precise concentrations were determined by amino acid analysis and used to calculate percent α-helical content as described previously (40).

RSV 5-HB. A 5-HB protein was designed containing 5 of the 6 helices that comprise the core of the RSV-F trimer of hairpins, connected by short peptide linkers in accordance with the design of the gp41 5-HB (33) (MAVSKVLHLEGEVNKIKSALLSTNKAVVSLSNGVSVLTSKV-LDLKNYIDKQLLPIVNKQGGSGGNFYDPLVFPSDEFDASISQVNEKIN-QSLAFIRKSDELLHNVNAGKGSSGGAVSKVLHLEGEVNKIKSALLSTN-

KAVVSLSNGVSVLTSKVLDLKNYIDKQLLPIVNKGGSGGNFYDPLVF-PSDEFDASISQVNEKINQSLAFIRKSDELLHNVNAGKGSSGGAVSKV-LHLEGEVNKIKSALLSTNKAVVSLSNGVSVLTSKVLDLKNYIDKQLL-PIVNKGGHHHHHH**). The plasmid (Genescript) was transformed into *Escherichia coli* BL21 (DE3), cultured in Luria broth, and induced with 0.1 M isopropyl β-D-thiogalactoside overnight at 37°C. The cells were harvested by centrifugation for 20 minutes at 5,000 *g*, resuspended in buffer A (100 mM NaH_2PO_4, 20 mM Tris, 8 M urea; pH 7.4), and lysed by agitation at 4°C overnight. The mixture was clarified by centrifugation (35,000 *g* for 30 minutes) before binding to a nickel-nitrilotriacetate (Ni-NTA) agarose (Qiagen) column at room temperature. The bound 5-HB was washed with buffer A (pH 6.3), eluted with buffer A (pH 4.5), renatured by diluting (1:2) with PBS (50 mM sodium phosphate, 100 mM NaCl; pH 7.5), and concentrated in a 10-kDa Amicon centricon (diluting and reconcentrating 7 times), yielding approximately 1 mg/ml protein solution. Purity of the protein was assessed by SDS-PAGE and determined to be >90%.

Fluorescence polarization assay. Fluoresceinated peptides (25 nM) were incubated with 5-HB protein at the indicated concentrations in room-temperature binding buffer (50 mM sodium phosphate, 100 mM NaCl; pH 7.5). Binding activity at 10 minutes was measured by fluorescence polarization using a SpectraMax M5 microplate reader (BMG Labtech). A fixed concentration of FITC-peptide and protein reflecting the EC_{90} for direct binding was then incubated with a serial dilution of acetylated SAH-RSVF peptide to generate competition curves for comparative analyses. Binding assays were run in triplicate, and K_is were calculated by nonlinear regression analysis of the competition binding isotherms using Prism software (GraphPad).

Fluorescence size exclusion chromatography. Fluorescent peptide and peptide/protein complex was resolved on an Agilent 1260 HPLC equipped with a fluorescence detector. A 100-μl solution of 500 nM FITC-$RSVF_{488–522}$ with or without 2 μM RSV 5-HB was injected onto a 10/100 GL Superdex 75 gel permeation column and eluted in 50 mM sodium phosphate buffer (pH 7.4) containing 150 mM NaCl using a flow rate of 0.5 ml/min.

Protease resistance assay. In vitro proteolytic degradation was measured by LC/MS (Agilent 1200) using the following parameters: 20 μl injection, 0.6 ml flow rate, 15-minute run time consisting of a gradient of water (0.1% formic acid) to 20%–80% acetonitrile (0.75% formic acid) over 10 minutes, 4-minute wash to revert to starting gradient conditions, and 0.5-minute post-time. The DAD signal was set to 280 nm with an 8-nm bandwidth and MSD set to scan mode with one channel at (M+2H)/2, ± 1 mass units, and the other at (M+3H)/3, ± 1 mass units. Integration of each MSD signal yielded areas under the curve of $>10^8$ counts. Reaction samples were composed of 5 μl peptide in DMSO (1 mM stock) and 195 μl buffer consisting of 50 mM $(NH_4)_2CO_3$, pH 7.4, for trypsin proteolysis or 50 mM Tris-HCl, pH 7.4, for proteinase K proteolysis. Upon injection of the 0-hour time sample, 2 μl of 50 ng/μl trypsin (Sigma-Aldrich) or 2.5 μl of 4 ng/μl proteinase K (New England Biolabs) was added, and the amount of intact peptide was quantitated by serial injection over time. A plot of MSD area versus time yielded an exponential decay curve, and half-lives were determined by nonlinear regression analysis using Prism software (GraphPad).

Mice. Female BALB/c mice (2–3 months old) were purchased from Harlan Laboratories.

Cell culture. HEp-2 cells (ATCC CCL 23) were used to propagate RSV and for viral plaque assays, and A549 cells (ATCC CCL-185) were used in RSV infectivity and syncytia formation assays. Cells were serially passaged in DMEM supplemented with 5% FBS and routinely tested for mycoplasma using the LookOut Mycoplasma PCR Detection Kit (Sigma-Aldrich).

Virus. rgRSV was obtained from M. Peeples (Nationwide Children's Hospital, Columbus, Ohio, USA), and the virus was propagated and plaques imaged as described previously (41). RSV-A2, an A-subtype RSV, was obtained from ATCC (catalog no. VR1302), and working stocks were prepared by infecting semiconfluent monolayers of mycoplasma-free HEp-2 cells. When the cells exhibited approximately 80% syncytia formation and substantial cytopathic effect (CPE), cells and medium from the monolayers were collected, pooled, and clarified by centrifugation (1,000 *g* at 4°C, 20 minutes). The supernatant was aliquoted, snap-frozen on dry ice, and stored at –80°C until use. The RSV-rA2Line19F strain and clinical isolate RSV 2-20 were gifts of M. Moore (Emory University, Atlanta, Georgia, USA) (34) and propagated in HEp-2 cells as described above for RSV-A2.

RSV infectivity assay. A549 cells were seeded in 24-well plates at 30,000 cells/well and the following day preincubated with the indicated SAH-RSVF peptides (5 μM) or vehicle for 30 minutes. rgRSV (0.1 MOI) was then added to the cells and allowed to infect for 1 hour at 37°C, followed by replacement of the medium with fresh medium containing SAH-RSVF peptides (5 μM). After 24 hours of infection, cells were harvested, and GFP^+ cells were quantitated by flow cytometry.

Syncytia formation assay. A549 cells were plated and treated as described above for the RSV infectivity assay. RSV infection produces characteristic cytopathic effects consisting of syncytia formation. After 48 hours of infection, syncytia were counted in 3 replicate wells per treatment at 4 different locations per well.

Plaque assay. A549 cells were plated and treated with the indicated SAH-RSVF peptides or vehicle as described above for the RSV infectivity assay, except that cells were infected with RSV-A2, RSV 2-20, or RSV-rA2Line19F strains at 0.1 MOI. Cell supernatants were collected for determination of viral titers (pfu/ml), and serial dilutions were used to infect 80% confluent HEp-2 cells in a 24-well plate, as described previously (42). After 1 hour of infection at 37°C with frequent rocking, the medium was replaced with complete overlay growth medium containing 0.8% methylcellulose and penicillin/streptomycin/amphotericin B. Plaques were immunostained 5 days after infection with monoclonal mouse anti–RSV-F antibody (AbD-Serotec, MCA490), followed by a horseradish peroxidase–conjugated anti-mouse secondary antibody, and visualized with 4CN substrate (Kirkegaard and Perry Laboratories Inc.). For the in vivo studies, the cranial lobe of the right lung was excised, weighed, and homogenized in DMEM (Invitrogen). Tissue debris was pelleted by centrifugation at 4°C for 10 minutes at 300 *g*, and supernatants were immediately serially diluted in FBS-free medium. Homogenates were clarified by centrifugation (5,000 *g*, 10 minutes), supernatants were collected, and viral titers were then determined as described above for HEp-2 cells.

RSV-N expression analysis. For RSV-N expression analysis in cultured cells, A549 cells were plated (10^6 cells/well) in a 6-well plate and treated with the indicated SAH-RSVF peptides or vehicle as described for the RSV infectivity assay, except that cells were infected with RSV-A2 at 0.1 MOI. Cell pellets were collected for analysis after 24 hours of infection. For RSV-N expression analysis in lung tissue, the caudal lobe of the right lung was removed and snap frozen. The A549 cell pellets and lung caudal lobes were homogenized in 1 ml TRIzol reagent (Invitrogen) according to the manufacturer's instructions, and 5 μg total RNA from each specimen was reverse transcribed to assess RSV-N expression. Hypoxanthine-guanine phosphoribosyltransferase (*HPRT*) was analyzed as an internal control; gene expression was normalized to *HPRT*. Fold changes in gene expression levels were calculated relative to gene expression in uninfected controls, which were assigned an arbitrary value of 1. RSV transcripts were amplified using SYBR green in a Bio-Rad, CFX96 Real time system by adapting previously reported primer sets (34, 43).

Fluorescence microscopy. A549 cells were plated in a 35-mm fluorodish (30,000 cells/dish). RSV-A2 (1.6×10^6 pfu/ml, 300 μl) was stained with 0.3 nM R-18 (Molecular Probes) for 1 hour, followed by passage through a Sephadex column as described previously (44, 45). FITC-labeled

SAH-RSVF$_b$ peptide was added to the cells first (1 μM), immediately followed by mixing of stained virus (150 μl) with growth medium (750 μl) and addition to the cell culture. Cells were imaged at 2 hours with a 4D live imaging system (Lisa Muma Weitz Advanced Microscopy and Cell Imaging Core Laboratory, University of South Florida).

Immunogold electron microscopy. A549 cells were grown to near confluence in T-75 flasks (USA Scientific), treated with FITC-labeled SAH-RSVF$_b$ peptide (5 μM), simultaneously infected with 0.1 MOI rA2-His$_6$-NS1, and harvested 1 hour after infection. Cells were pelleted and processed, and sections were gold-labeled on nickel grids as described previously (46). Briefly, grids were treated with 25 μl TBS-supplemented buffer (0.05 M Tris, 0.85% NaCl, pH 8.3–8.5, 0.5% normal goat serum, 0.5% normal pig serum, 0.5% BSA) with 3% nonfat dry milk for 2 hours at room temperature. Grids with thin sections were incubated with 50 μl anti-FITC rabbit antibody (1:100 dilution) diluted in TBS-supplemented buffer with 3% nonfat dry milk for 3 hours at room temperature, washed, and stained with the anti-rabbit antibody conjugated with 15 nm gold (Ted Pella Inc.) for 1 hour at room temperature. Grids were washed thoroughly and then treated with 1:20 dilution of 5 nm gold–Ni-NTA (Molecular Probes). After stream washing and 3 washes with distilled water (10 minutes each), grids were dried, stained with 2% aqueous uranyl acetate for 5 minutes, and examined on a JOEL 1200 EX scanning/transmission electron microscope at 80 kV.

Viral fusion assay. RSV-A2 virus (10 pfu/cell in 300 μl) was simultaneously labeled with DiOC18 and R18 (Invitrogen) as described previously (35, 44). The dyes were added to the viral suspension, mixed vigorously, and then gently shaken for an additional 1 hour at room temperature in the dark. Unbound dye was removed by gel filtration using a G-50 Macrospin column (Harvard Apparatus). A549 cells were seeded in an 8-well chambered slide (15,000 cells/well) overnight; the next day, cells (80% confluence) were washed with ice-cold PBS, then incubated with dual-labeled virus combined with vehicle or 10 μM SAH-RSVF$_{BD}$ peptide at 4°C for a 30-minute attachment period. For the final 10 minutes of the attachment stage, Cell Mask deep red plasma membrane marker (5 μg/ml; Invitrogen) was added to the cell culture. The 8-well chambered slide was then placed on a microincubator maintained at 37°C and imaged using a 3i Olympus Spinning Disk Confocal Microscope (Lisa Muma Weitz Advanced Microscopy and Cell Imaging Facility, University of South Florida). 5 different positions per well were imaged every 10 minutes for 2 hours. The number of fusion events, as reflected by a shift in the fluorescence emission of virions at 555–618 nm from red to orange-yellow or green, was counted for 25 cells per captured image in 5 different positions at 12 time points.

In vivo model of rgRSV infection and intranasal prophylactic treatment. 10-week-old BALB/c mice (n = 8) were anesthetized and treated intranasally with the indicated SAH-RSVF peptides (125 μM in 1.2% DMSO) or volume-equivalent vehicle (n = 2 per group). 1 hour after treatment, 3 groups of mice were inoculated with a single dose of virus at 1×10^6 pfu/mouse, with the fourth group receiving a mock inoculation. Mice were sacrificed 24 hours after infection, and the noses were harvested, sectioned, stained with DAPI, and imaged with an Olympus fluorescent microscope. Sections were also stained with H&E (Fisher) according to the manufacturer's protocol. The entire experiment was repeated, yielding a total of 16 experimental mice (n = 4 per cohort).

In vivo model of RSV-A2 infection and intranasal prophylactic treatment. 10-week-old BALB/c mice (n = 16) were anesthetized and treated intransally with the indicated SAH-RSVF peptides (125 μM in 1.2% DMSO) or volume-equivalent vehicle (n = 4 per group). 1 hour after treatment, 3 groups of mice were inoculated with a single dose of RSV-A2 at 1×10^6 pfu/mouse. The fourth group was treated with volume-equivalent vehicle and mock infected. Mice were sacrificed 4 days after treatment, the chest cavity was opened, and the left lung was gently perfused intratracheally with chilled 4% paraformaldehyde in PBS. The lung was then removed and immersed in 4% paraformaldehyde for an additional 6 hours. An equal volume of 30% sucrose in PBS was added, and tissues were fixed overnight at 4°C. The next day, the solution was replaced with 30% sucrose in PBS, and tissues were maintained at 4°C for an additional 24 hours. Fixed tissues were gently blotted, embedded in OCT, and then snap frozen on dry ice. Sections (5 μm) were treated with 1:1,000 dilution of rabbit anti-RSV polyclonal antibody (Millipore) overnight followed by anti-rabbit antibody conjugated to Alexa Fluor 555 (1:400) (red) (Molecular Probes) for 1 hour. Sections were then washed, mounted with medium containing DAPI (blue), and viewed with an Olympus fluorescent microscope. Cranial and caudal lobes of the right lung were snap frozen separately on dry ice. Lung homogenates were made from the cranial lobe, and the supernatants were used to determine viral titers by plaque assay on Hep-2 cells ($\log_{10}$ pfu/ml). Total RNA was isolated from the caudal lobe using RNeasy mini kit (Qiagen), and quantitative RT-PCR was performed for the RSV-N gene, as described above. This in vivo study was also performed with repeat peptide dosing and viral inoculation 16 hours after the initial infection (n = 3 per cohort).

SAH-RSVF peptide NP preparation and intratracheal administration. A stock solution (10 mg/ml) of soluble chitosan (30 kDa) was prepared in water. 1 volume of SAH-RSVF peptide and 2.5 volumes of chitosan were mixed in a microfuge tube to a final volume of 50 μl, and then vortexed on a digital vortex mixer for 15 minutes (200 *g*) at room temperature prior to administration. 10-week-old BALB/c mice (n = 6) were anesthetized and inoculated intratracheally with a 50 μl volume of 100 μM Cy5-labeled SAH-RSVF$_{BD}$ peptide with or without NP (1:2.5 peptide/NP ratio) or volume-equivalent vehicle (n = 2 per group). Mice were sacrificed 24 hours after treatment, and lungs were harvested after 1% paraformaldehyde perfusion, followed by cryopreservation in OCT. Sections (5 μm) were mounted in DAPI-containing medium and imaged with an Olympus fluorescent microscope.

In vivo model of RSV-rA2Line19F infection and intratracheal prophylactic treatment. 10-week-old BALB/c mice (n = 15) were anesthetized and inoculated intratracheally with a 50 μl volume of SAH-RSVF$_{BD}$ alone (250 μM peptide in 1.2% DMSO), SAH-RSVF$_{BD}$ combined with NP (1:2.5 peptide/NP ratio), NP with volume-equivalent vehicle, or volume-equivalent vehicle alone (n = 3 per group). 48 hours after treatment, the 4 groups of mice were inoculated intranasally with a single dose of clinical isolate RSV-rA2Line19F at 1×10^6 pfu/mouse. A fifth treatment group (n = 3) received volume-equivalent vehicle intratracheally followed by mock inoculation 48 hours later. Mice were sacrificed 4 days after infection, and right and left lung lobes were harvested as described above for immunofluorescence imaging, H&E staining, and determination of viral titers and RSV-N expression level, performed as described above. The entire experiment was repeated as above, except that intranasal inoculations were performed 72 hours after peptide treatment.

Quantitation of RSV$^+$ cells by ImageJ analysis. Immunofluorescence images were converted to binary 8-bit formats, and maximal points were quantified in areas surrounding bronchioles after noise and background were minimized using the Image-based Tool for Counting Nuclei (ITCN) ImageJ plugin. Nonspecific Ig antibody was used to determine background fluorescence, which was subtracted prior to image acquisition. 5 areas per microscopic field were quantified, and at least 8 images per mouse were collected. 2-way ANOVA of count averages was performed using Minitab software.

Statistics. Statistical analyses (1-way ANOVA followed by Bonferroni's multiple comparison test, or 2-tailed unpaired t test) were performed using GraphPad Prism software. A P value less than 0.05 was considered significant.

Study approval. All animal experiments were approved by and performed in accordance with the University of South Florida and Veterans' Affairs Hospital IACUC.

Acknowledgments

We thank E. Smith for assistance with figure preparation and M. Moore for providing the engineered RSV strains and clinical isolate 2-20. This work was supported in part by NIH grant 5R01 AI084102 and a Burroughs Wellcome Fund Career Award in the Biomedical Sciences to L.D. Walensky, a Research Career Scientist Award and VA Merit Review Award 5I01BX000954-02 by the Department of Veteran Affairs and NIH grant 1P30HL101265-01 to S.S. Mohapatra, and a University of South Florida Signature Research Program Fellowship to T. Wong. This study is based on work supported in part by the Department of Veterans Affairs, Veterans Health Administration, Office of Research and Development; the contents of this report do not represent the views of the Department of Veterans Affairs or the United States Government.

Received for publication June 28, 2013, and accepted in revised form January 23, 2014.

Address correspondence to: Loren D. Walensky, Dana-Farber Cancer Institute, 450 Brookline Avenue, Mayer 664, Boston, Massachusetts 02215, USA. Phone: 617.632.6307; Fax: 617.582.8240; E-mail: loren_walensky@dfci.harvard.edu. Or to: Shyam S. Mohapatra, James A. Haley VA Hospital, 13000 Bruce B. Downs Boulevard, Tampa, Florida 33612, USA. Phone: 813.974.8568; Fax: 813.974.8575; E-mail: shyam.mohapatra@va.gov.

1. Initiative for Vaccine Research. *Acute Respiratory Infection*. Geneva, Switzerland: World Health Organization; 2009.
2. Karron RA. Respiratory syncytial virus and parainfluenza virus vaccines. In: Plotkin SA, Orenstein WA, Offit PA, eds. *Vaccines*. 5th ed. New York, New York, USA: Saunders Elsevier; 2008:1283–1293.
3. Thompson WW, et al. Mortality associated with influenza and respiratory syncytial virus in the United States. *JAMA*. 2003;289(2):179–186.
4. Falsey AR, Walsh EE. Respiratory syncytial virus infection in adults. *Clin Microbiol Rev*. 2000;13(3):371–384.
5. Han LL, Alexander JP, Anderson LJ. Respiratory syncytial virus pneumonia among the elderly: an assessment of disease burden. *J Infect Dis*. 1999; 179(1):25–30.
6. Mullooly JP, et al. Influenza- and RSV-associated hospitalizations among adults. *Vaccine*. 2007; 25(5):846–855.
7. Falsey AR, Walsh EE. Respiratory syncytial virus infection in elderly adults. *Drugs Aging*. 2005;22(7):577–587.
8. Centers for Disease Control and Prevention (CDC). Respiratory syncytial virus activity — United States, 1999–2000 season. *MMWR Morb Mortal Wkly Rep*. 2000;49(48):1091–1093.
9. Silva A, Erickson JE, Eissenstat M, Afonina E, Gulnik, S, inventors; Sequoia Pharmaceuticals, assignee. Long acting biologically active conjugates. US patent 10/550,715. March 24, 2003.
10. Hall CB, et al. Respiratory syncytial viral infection in children with compromised immune function. *N Engl J Med*. 1986;315(2):77–81.
11. Lambert DM, et al. Peptides from conserved regions of paramyxovirus fusion (F) proteins are potent inhibitors of viral fusion. *Proc Natl Acad Sci U S A*. 1996;93(5):2186–2191.
12. Pastey MK, Gower TL, Spearman PW, Crowe JE, Crowe JE Jr, Graham BS. A RhoA-derived peptide inhibits syncytium formation induced by respiratory syncytial virus and parainfluenza virus type 3. *Nat Med*. 2000;6(1):35–40.
13. Shepherd NE, Hoang HN, Desai VS, Letouze E, Young PR, Fairlie DP. Modular alpha-helical mimetics with antiviral activity against respiratory syncitial virus. *J Am Chem Soc*. 2006;128(40):13284–13289.
14. Cianci C, Meanwell N, Krystal M. Antiviral activity and molecular mechanism of an orally active respiratory syncytial virus fusion inhibitor. *J Antimicrob Chemother*. 2005;55(3):289–292.
15. Douglas JL, et al. Inhibition of respiratory syncytial virus fusion by the small molecule VP-14637 via specific interactions with F protein. *J Virol*. 2003; 77(9):5054–5064.
16. Olszewska W, et al. Antiviral and lung protective activity of a novel respiratory syncytial virus fusion inhibitor in a mouse model. *Eur Respir J*. 2011;38(2):401–408.
17. Razinkov V, Gazumyan A, Nikitenko A, Ellestad G, Krishnamurthy G. RFI-641 inhibits entry of respiratory syncytial virus via interactions with fusion protein. *Chem Biol*. 2001;8(7):645–659.
18. Roymans D, et al. Binding of a potent small-molecule inhibitor of six-helix bundle formation requires interactions with both heptad-repeats of the RSV fusion protein. *Proc Natl Acad Sci U S A*. 2010;107(1):308–313.
19. Kumar M, et al. Intranasal gene transfer by chitosan-DNA nanospheres protects BALB/c mice against acute respiratory syncytial virus infection. *Hum Gene Ther*. 2002;13(12):1415–1425.
20. Kumar M, Behera AK, Matsuse H, Lockey RF, Mohapatra SS. Intranasal IFN-γ gene transfer protects BALB/c mice against respiratory syncytial virus infection. *Vaccine*. 1999;18(5–6):558–567.
21. Zhang W, et al. Inhibition of respiratory syncytial virus infection with intranasal siRNA nanoparticles targeting the viral NS1 gene. *Nat Med*. 2005; 11(1):56–62.
22. Garg R, Latimer L, Simko E, Gerdts V, Potter A, van den Hurk Sv. Induction of mucosal immunity and protection by intranasal immunisation with a novel respiratory syncytial virus vaccine formulation. *J Gen Virol*. 2014;95(pt 2):301–306.
23. McLellan JS, et al. Structure of RSV fusion glycoprotein trimer bound to a prefusion-specific neutralizing antibody. *Science*. 2013;340(6136):1113–1117.
24. Stab V, et al. Protective efficacy and immunogenicity of a combinatory DNA vaccine against Influenza A Virus and the Respiratory Syncytial Virus. *PLoS One*. 2013;8(8):e72217.
25. McLellan JS, et al. Structure-based design of a fusion glycoprotein vaccine for respiratory syncytial virus. *Science*. 2013;342(6158):592–598.
26. Zhao X, Singh M, Malashkevich VN, Kim PS. Structural characterization of the human respiratory syncytial virus fusion protein core. *Proc Natl Acad Sci U S A*. 2000;97(26):14172–14177.
27. Melikyan GB. Common principles and intermediates of viral protein-mediated fusion: the HIV-1 paradigm. *Retrovirol*. 2008;5:111.
28. Kilby JM, et al. Potent suppression of HIV-1 replication in humans by T-20, a peptide inhibitor of gp41-mediated virus entry. *Nat Med*. 1998;4(11):1302–1307.
29. Lawless-Delmedico MK, et al. Heptad-repeat regions of respiratory syncytial virus F-1 protein form a six-membered coiled-coil complex. *Biochemistry*. 2000; 39(38):11684–11695.
30. Schafmeister CE, Po J, Verdine GL. An all-hydrocarbon cross-linking system for enhancing the helicity and metabolic stability of peptides. *J Am Chem Soc*. 2000;122:5891–5892.
31. Walensky LD, et al. Activation of apoptosis in vivo by a hydrocarbon-stapled BH3 helix. *Science*. 2004;305(5689):1466–1470.
32. Bird GH, et al. Hydrocarbon double-stapling remedies the proteolytic instability of a lengthy peptide therapeutic. *Proc Natl Acad Sci U S A*. 2010; 107(32):14093–14098.
33. Root MJ, Kay MS, Kim PS. Protein design of an HIV-1 entry inhibitor. *Science*. 2001;291(5505):884–888.
34. Moore ML, et al. A chimeric A2 strain of respiratory syncytial virus (RSV) with the fusion protein of RSV strain line 19 exhibits enhanced viral load, mucus, and airway dysfunction. *J Virol*. 2009; 83(9):4185–4194.
35. Sakai T, et al. Dual wavelength imaging allows analysis of membrane fusion of influenza virus inside cells. *J Virol*. 2006;80(4):2013–2018.
36. Bolger G, et al. Primary infection of mice with high titer inoculum respiratory syncytial virus: characterization and response to antiviral therapy. *Can J Physiol Pharmacol*. 2005;83(2):198–213.
37. Sudo K, Watanabe W, Mori S, Konno K, Shigeta S, Yokota T. Mouse model of respiratory syncytial virus infection to evaluate antiviral activity in vivo. *Antivir Chem Chemother*. 1999;10(3):135–139.
38. Takeshita T, et al. Effect of brazilian propolis on exacerbation of respiratory syncytial virus infection in mice exposed to tetrabromobisphenol a, a brominated flame retardant. *Evid Based Complement Alternat Med*. 2013;2013:698206.
39. Bird GH, Crannell CW, Walensky LD. Chemical synthesis of hydrocarbon-stapled peptides for protein interaction research and therapeutic Targeting. *Curr Protoc Chem Biol*. 2011;3(3):99–117.
40. Bird GH, Bernal F, Pitter K, Walensky LD. Synthesis and biophysical characterization of stabilized alpha-helices of BCL-2 domains. *Methods Enzymol*. 2008;446:369–386.
41. Hallak LK, Collins PL, Knudson W, Peeples ME. Iduronic acid-containing glycosaminoglycans on target cells are required for efficient respiratory syncytial virus infection. *Virology*. 2000;271(2):264–275.
42. Bitko V, Musiyenko A, Shulyayeva O, Barik S. Inhibition of respiratory viruses by nasally administered siRNA. *Nat Med*. 2005;11(1):50–55.
43. Perkins SM, et al. Comparison of a real-time reverse transcriptase PCR assay and a culture technique for quantitative assessment of viral load in children naturally infected with respiratory syncytial virus. *J Clin Microbiol*. 2005;43(5):2356–2362.
44. San-Juan-Vergara H, et al. Cholesterol-rich microdomains as docking platforms for respiratory syncytial virus in normal human bronchial epithelial cells. *J Virol*. 2012;86(3):1832–1843.
45. San-Juan-Vergara H, Peeples ME, Lockey RF, Mohapatra SS. Protein kinase C-alpha activity is required for respiratory syncytial virus fusion to human bronchial epithelial cells. *J Virol*. 2004;78(24):13717–13726.
46. Boyapalle S, Wong T, Garay J, Teng M, San Juan-Vergara H, Mohapatra S. Respiratory syncytial virus NS1 protein colocalizes with mitochondrial antiviral signaling protein MAVS following infection. *PLoS One*. 2012;7(2):e29386.